Meta-foam Numerical Optimization for Surface Enhanced Solar Steam Generation

Lan Gao, Yamin Leprince-Wang, Tarik Bourouina, E. Nefzaoui

META-FOAM NUMERICAL OPTIMIZATION FOR SURFACE-ENHANCED SOLAR STEAM GENERATION

Lan Gao, Yamin Leprince-Wang, Tarik Bourouina, Elyes Nefzaoui*
ESYCOM Lab, Univ Gustave Eiffel, CNRS, F-77454 Marne-la-Vallée, France

ABSTRACT

Enhanced solar steam generation is a promising process for water purification. Evaporation efficiency can be increased by localizing heating process at the water-air interface using photothermal materials. As of late, numerous black absorber sheets (BAS) have been developed, which can be seen as meta-foams with micro/nanostructured porous media exhibiting remarkable properties in terms of solar radiation-to-heat conversion to achieve efficient steam generation. By taking advantage of the porous structure of the BAS, both thermal insulation and stable water capillary transport functions are simultaneously achieved by the same material. Water heating is therefore concentrated only at the surface, which increases the evaporation efficiency up to 85% under 1 sun illumination. In this contribution, we report on theoretical modeling and numerical simulations of BAS-assisted steam generation to guide the optimization of BAS regarding the maximization of the evaporation rate. Numerical simulations are performed using multi-physical simulation tools to simultaneously account for heat and mass transfer including photo-thermal conversion, capillary transport and water phase change. Parametric studies are also conducted to determine the key parameters for an optimized BAS maximizing steam generation rate. Considered parameters include the porosity ε and the surface absorptivity α of BAS. An optimal porosity of 0.75 is found to maximize the evaporation rate. We also report on the observed trend of the evaporation rate with respect to key parameters of the BAS structure.

KEY WORDS: solar energy, steam generation, porous media, evaporation rate

1. INTRODUCTION

Solar distillation is considered to be one of the most effective approaches for water purification [1–5]. The utilization of solar energy makes it possible for the water purification process to be environmentally friendly. On the other hand, the required facilities and equipment for this process are relatively easy to install and operate. For these reasons, solar distillation technology has drawn the attention of many research groups over the past few decades. To achieve high efficiency solar distillation, several solutions have been proposed such as pre-heated methods [6,7], nocturnal heated methods [8,9]or methods coupled with additional heat sources to increase the system operating temperature [10–13]. Enhanced Solar Steam Generation (SSG) with a Black Absorber Sheet (BAS) is one of these methods [14]. As the evaporation only occurs at the air-water interface, with the help of a BAS, steam generation efficiency can be increased by localizing the heating process at this interface and reducing the water reservoir bulk heating.

*Corresponding Author: elyes.nefzaoui@univ-eiffel.fr

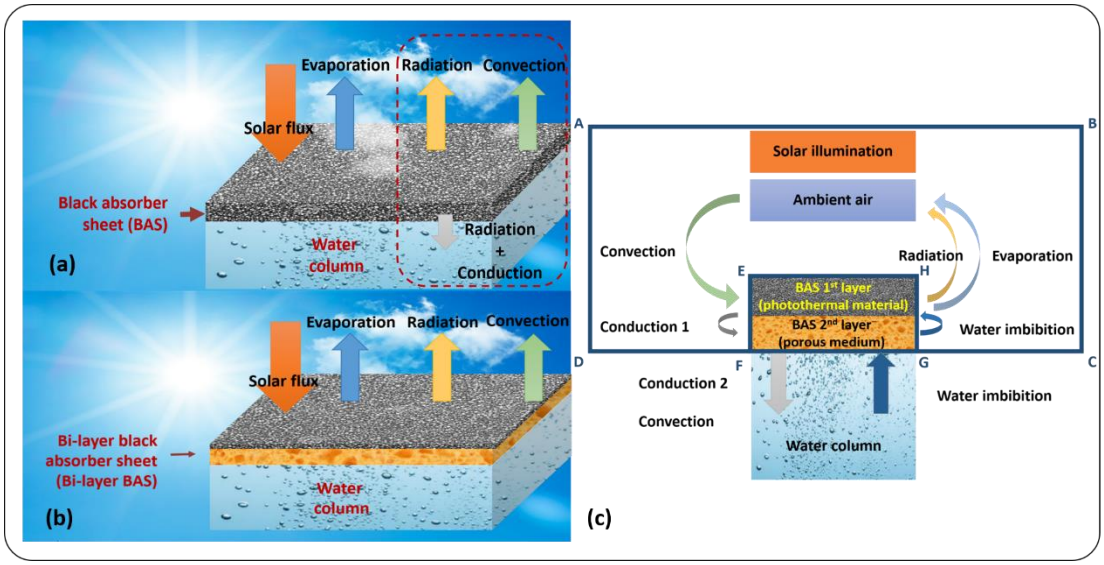

Fig. 1*:* Enhanced solar steam generation system schematic with single layer (a) and bi-layer (b) BAS showing the different heat transfer phenomena involved. (c) Schematic of a bi-layer BAS-enhanced steam generation device component geometry in the COMSOL model and involved physical phenomena.

It has been experimentally proven recently that a micro-scale porous-structured BAS improves the SSG efficiency by switching from bulk heating to surface heating [14]. As shown in Fig. 1 (a), the BAS plays two key roles: on one hand, localized heating because of the BAS high absorptivity and low thermal conductivity, on the other hand, water imbibition by capillary effect in the BAS porous structure. In the simple case of a single layer BAS, these two functionalities are ensured by the same material. A more sophisticated strategy, shown in Fig. 1 (b); uncouples the two functionalities has been recently proposed as a bi-layer BAS SSG; it shows and improved steam generation efficiency [15]. The top layer is a high absorptivity photothermal layer where light-to-heat conversion is localized. The second and bottom layer is a low thermal conductivity porous media which ensures water imbibition and reduces heat loss into the water column. Discussion of some theoretical aspects of bi-layer BAS have been recently reported. The water imbibition velocity which relies on the capillary effect in the porous media has been modeled as a function of the porous layer properties. The energy conversion process during water evaporation is also discussed. With a controlled ambient airflow velocity, the maximal enhanced steam generation rate has been calculated and the effect of some physical parameters such as the surface absorptivity of the top layer has been discussed [16,17]. However, modeling of the entire system and a systematic discussion of the role of the different BAS properties have not been performed yet. In this study, we report on a comprehensive theoretical and numerical study of BAS-assisted enhanced SSG accounting for coupled heat transfer as well as mass transfer in the porous media, evaporation at water-air interface and water vapor transport in air. A parametric study with respect to key physical parameters is also performed using the developed numerical model to guide the optimization of BAS for enhanced SSG.

The paper is constructed as follows: In section 2, we present the principle of a bilayer BAS-assisted SSG as well as the used analytical and numerical model. In section 3, we present the main results and discuss the system performances with respect to key parameters such as the ambient air relative humidity (RH), the BAS absorptivity and porosity and the used materials thermal conductivity before summarizing the main results and perspectives in the concluding section.

2. MATERIALS AND METHODS

1.1. **Bi-layer BAS-enhanced solar steam generation system**

We illustrate in Fig. 1 (c) the different physical phenomena governing energy and mass transport in a bi-layer BAS-enhanced SSG. First, incident radiation is absorbed by the BAS top layer. This layer absorptivity is the key parameter in this first step. Its thermal conductivity is also of paramount importance if we target heat generation concentration at the device surface. This layer heat capacity has also to be considered if we consider the device in transient regime. The BAS second layer is used for two purposes: (i) liquid water transport from the reservoir, i.e. the water column, to the hot spot at the device surface designed as the evaporation site; and (ii) thermal insulation to prevent heat transport to the water reservoir and maximize temperature at the device surface.
Considering these two goals, many parameters play a key role in this second layer: porosity for water mass transport and porosity and thermal conductivity for thermal insulation. Heat capacity has also to be considered if we consider transient regime operation, which is not the case in the present work. The porous material media of this second layer is assumed to be a uniform mixture of air and a solid material. In transient operation, the time required for water rising up to the porous media surface is much smaller than the time required for the entire system to reach equilibrium [18,19]. Therefore, we assume that the porous media is always saturated, which means evaporation is not limited by water imbibition. Thermo-physical properties of the porous media strongly depend on the solid material properties and the porous structure. In this study, we use a simple Effective Thermal Conductivity (ETC) model to obtain the thermo-physical properties of the BAS [20,21] as a volume weighed average of the thermal conductivities of the material constituents. To study the effect of materials properties on BAS-enhanced SSG, a numerical model implemented using COMSOL Multiphysics is used.

1.2. **Analytical model**

1.2.1. Energy balance and evaporation rate

Based on the physical model schematically depicted in Fig. 1 (a), the total energy input of the system is provided by the first photothermal layer, which absorbs the incident solar radiation and converts it into heat. Thus, the main driving quantity is the absorbed radiative heat flux q_{abs} that can be expressed as:

$$q_{abs} = \alpha q_{solar} \quad (1)$$

where, α is the first layer absorptivity and q_{solar} is the incident solar radiation set equal to 1000 W/m^2 under one sun illumination. If we account for the different governing phenomena described in Fig. 1, the energy balance for the entire system can be written as follows:

$$\alpha q_{solar} = q_{evap} + q_{conv} + q_{cond} + q_{rad} \quad (2)$$

where, q_{conv}, q_{cond}, q_{rad} are the convective, conductive and radiative heat flux respectively while q_{evap} is the heat flux required for water evaporation that can be written as follows:

$$q_{evap} = L_v \cdot \dot{m}_v \quad (3)$$

where, L_v is the latent heat of water evaporation and $\dot{m}_v$ is the evaporation rate. This first set of equations enables the calculation of the asymptotic limit of the evaporation rate using simplifying assumptions. Additional information on governing equations can be found in [22].

1.2.2. Heat and mass transfer in the porous media

In this layer, the transport of three different species takes place: liquid phase water, water vapor and airflow. The liquid phase water velocity is described by Darcy's law as a function of the vapor pressure

gradient [23]. We can also describe the capillary transport in the porous media as a diffusion process, in a similar manner than for water vapor transport, using empirical equations [24]. The effective diffusivity of water vapor is described by Millington and Quirk equation [25]. From Brinkman equation [26], the velocity field of water vapor is obtained as a combination of velocity fields resulting from both convection and water vapor diffusion. On the other hand, airflow in the porous media is described by Navier-Stokes equations, where the thermal properties of the porous media are taken into account [27,28]. One should note that the porous media content of different phases has a non-negligible impact on the porous media properties and heat transfer. Therefore, thermal properties of the BAS second layer are calculated as a weighted average of the properties of the different phase accounting for the fluids volume fraction ε and the bulk material volume fraction 1- ε [29–32].

Finally, for water vapor transport in ambient air, we assume the entire process is spontaneous and not assisted by forced convection for vapor evacuation. Therefore, water vapor transport in ambient air is ensured by species concentration diffusion and natural convection which results from the temperature difference between the BAS surface and the ambient air. Compared to previously reported works [17], we account for these two phenomena in our model by using laminar flow temperature-dependent compressible Navier-Stokes equations implemented in a multi-physical commercial simulation software.

1.3. **Numerical model**

To solve the equations described in the previous section, we modeled the system using COMSOL Multiphysics in a two-dimensional (2D) configuration. We show in Fig. 1 (c) the considered geometry where we can clearly distinguish a BAS block (EHGF) and an ambient air block (ABCD). The BAS block is 5 mm thick and 40 mm wide. It is nested in a larger air block which dimensions are 250 x 250 mm^2. To simplify the model, we make the following assumptions: (1) The thickness of the BAS first layer is negligible compared to the total thickness of the BAS; (2) Radiative losses are located in the first layer of the BAS only; (3) The porous media of the BAS second layer is isotropic; (4) Ambient air humidity is constant, hence not affected by generated steam. This requires an efficient evacuation of water vapor from the BAS surface; (5) Only natural convection is accounted for at the BAS surface. Boundary conditions used for simulation are listed in Table **Table 1**.

Table 1 : Numerical simulations boundary conditions

Case	Diameter, d_B [mm]	f [Hz]	*We*	*St*
AB	Open boundary	Open boundary	unrelated	Open boundary
AD	Open boundary	Open boundary	unrelated	Open boundary
BC	Open boundary	Open boundary	unrelated	Open boundary
DE	Open boundary	Open boundary	unrelated	Open boundary
HC	Open boundary	Open boundary	unrelated	Open boundary
EF	Wall	No flux	No flux	No flux
EH	Coupling boundary	-n·q = α qsolar	No flux	Coupling boundary
HG	Wall	No flux	No flux	No flux
GF	Wall	No flux	Inlet	No flux

A time-dependent simulation has been performed. The related variables are listed in Table S3 (supplementary materials).

3. RESULTS AND DISCUSSION

In this section, we present the main results obtained using the analytical and numerical models introduced in the previous sections. First, using the analytical model, we calculate the ultimate evaporation rate that can be obtained in enhanced SSG under direct solar radiation and ideal conditions. Then, we use the numerical model to study the effect of key parameters on enhanced SSG performances including the humidity of ambient air, the top layer absorptivity, the BAS second layer porosity as well as the second layer material thermal conductivity. Optimal properties are obtained and discussed with respect to the properties of common materials that can be used for this application.

1.1. **Asymptotic limit of the evaporation rate**

If we assume an ideal BAS-assisted enhanced SSG system operating in steady state, where all thermal losses (convective, conductive and radiative) are neglected and where all incident solar radiation is absorbed and exclusively used for water evaporation, the combination of equations 1, 2 and 3 leads to:

$$\dot{m}_v = \frac{q_{solar}}{L_v} \qquad (4)$$

where, $\dot{m}_v$ is the generated vapor mass flow rate per unit surface area, $L_v = 2453.6\ \mathrm{kJ/kg}$ is vaporization latent heat (we consider a constant ambient temperature T = 293.15 K and an evaporation temperature of T = 313.15 K) and q_{solar} = 1000W/m^2.

Using these different assumptions, we obtain an evaporation rate of 1.511 kg/(h·m^2). This value is the maximal evaporation rate that can be obtained with an ideal enhanced SSG system when solar radiation harvesting is maximized and all losses minimized. We note that this value is one or two orders of magnitude lower than values of the capillary flow rate that can be obtained using common porous media [33], also meaning that capillary flow-rate is not a limiting factor. This result also confirms that the evaporation rate is mainly limited by the energy input of the system and thermal losses which are the bottleneck to be optimized.

In the following paragraphs, we discuss using a parametric study the effect of other parameters that may affect an SSG system performance.

1.2. **Effect of ambient air relative humidity on the evaporation rate**

A parametric study of SSG is performed by varying different ambient conditions, in particular the ambient air humidity. In each simulation of the parametric sweep, we consider constant ambient air humidity during the SSG process, which can be assumed if SSG occurs in a strictly controlled environment or if the volume around the SSG system is large enough compared to the injected vapor volume (in the case of an outdoor experiment for example) to ensure that evaporation does not change the surrounding environment humidity. Obtained results are plotted in Fig. 2. The evaporation rate gradually decreases from 1.05 kg/(h·m^2) to 0.97 kg/(h·m^2) as the RH increases from 0 to 0.5 when the surface absorptivity is 0.9 and the porosity is 0.7.

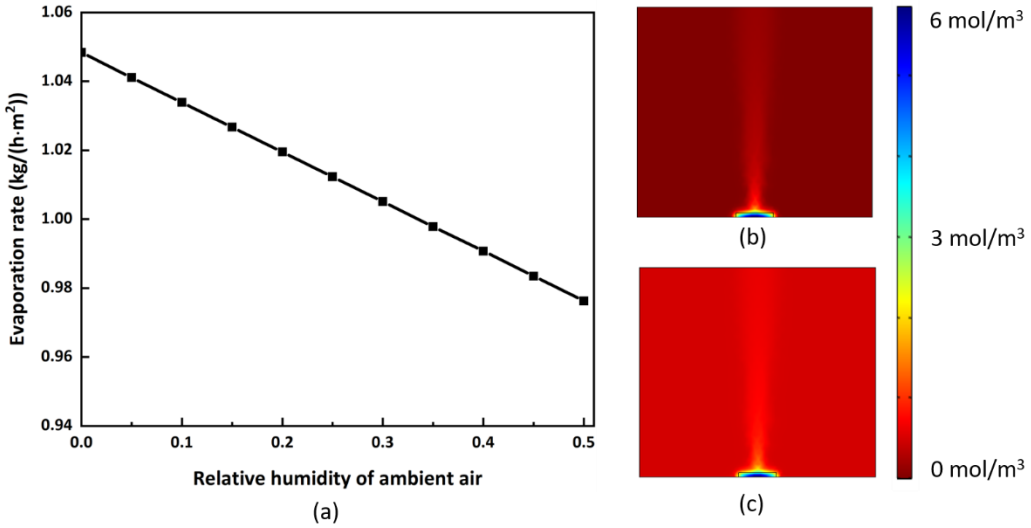

Fig. 2: (a) Evaporation rate as a function of ambient air humidity, (b) Water vapor concentration field in the system at an ambient RH of 0 and (c) Water vapor concentration field in the system at an ambient RH of 0.5.

1.3. **Effect of surface absorptivity**

In a BAS-enhanced SSG system, *the BAS top layer* surface absorptivity is the first key parameter for the system operation since it governs the light-to-heat conversion process of BAS and therefore determines the total energy input to the system. We plot in the Fig. 3 BAS equilibrium temperature and the evaporation flow rate as a function of the surface absorptivity as computed using the multi-physical numerical model. Plotted results indicate that the higher the absorptivity the higher the evaporation rate. The evaporation rate increases almost linearly from 0.50 kg/(h·m^2) to 0.72 kg/(h·m^2) as the absorptivity increases from 0.3 to 1 with a porosity of 0.9 using polyurethane material. Temperature fields in the system are also shown in Fig. 3. The maximum temperature is obtained at the top surface of the BAS which is expected since this spot is designed as the evaporation site. The BAS top surface temperature also increases gradually form 309.15 K to 325.15 K as the surface absorptivity increase from 0.5 to 0.9 while the simulation temperature initial condition of the BAS and entire system are set to be 293.15 K.

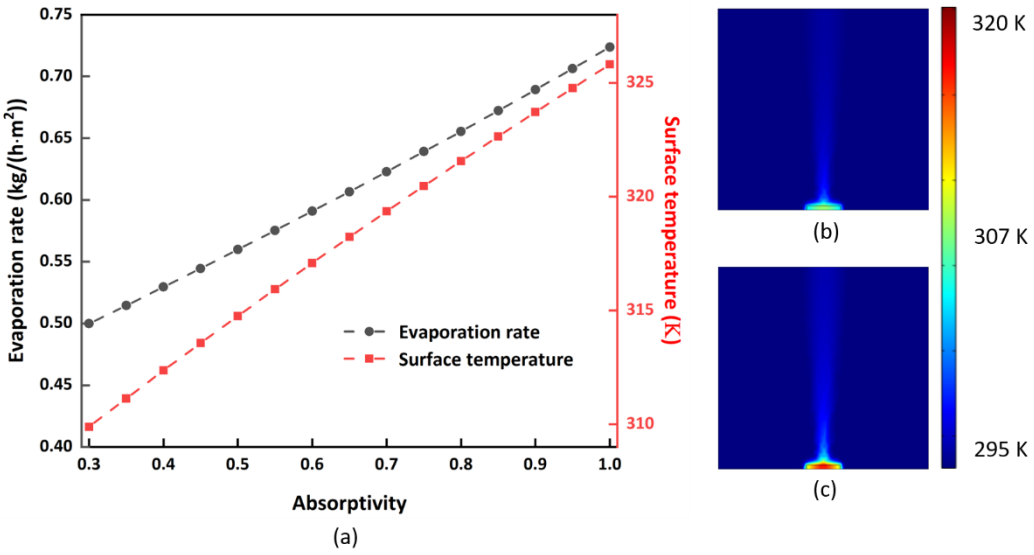

Fig. 3: (a) The BAS surface temperature at thermal equilibrium as a function of the BAS top layer absorptivity and the temperature field in the system at equilibrium for an absorptivity of (b) 0.3 and (c) 0.9.

The simultaneous increase of equilibrium temperature and evaporation rate can be explained by the dependence of evaporation latent heat to temperature. This quantity actually decreases with temperature going from 2453.6 kJ/kg at 293 K up to 2256.4 kJ/kg at 373 K. Consequently, a further increase in the BAS surface temperature would lead to an additional increase of the evaporation rate. However, the larger the surface temperature the larger the heat loss to ambient air and the input energy required to maintain the BAS top layer temperature. Such additional increase in temperature and the evaporation rate could be achieved by a strong thermal insulation of the BAS top layer.

1.4. **Effects of porosity**

The porosity ε is the main key parameter in the second layer of BAS since it governs both BAS thermal conductivity, hence heat transport from BAS surface to the water column, and liquid water transport from the liquid column to the BAS surface. A parametric study is conducted in which porosity is varied from 0.3 to 0.9 with different values of the surface absorptivity α. Results are shown in Fig. 4 and Fig. 5. By comparing the concentration fields in Fig. 4 (a) and (b), we can observe a significant increasing of the water vapor concentration when the porosity increasing from 0.3 to 0.75. At the same time, the temperature fields in Fig. 4 (c) and (d) indicate that the maximum temperature in the system decreases as the porosity increases from 0.3 to 0.75. By comparing the results of porosity at 0.3 and 0.75 regarding the temperature field and the water vapor concentration, it's worth mentioning that the evaporation rate of 0.75 has a higher evaporation rate than the porosity of 0.3 even though with lower surface temperature.

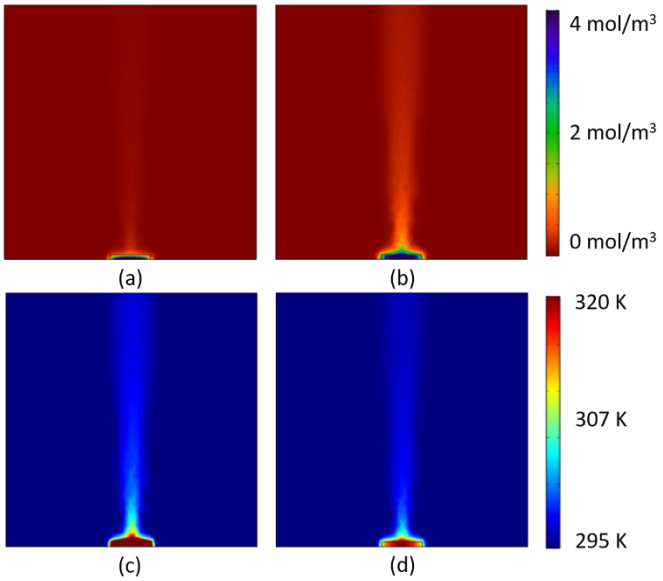

Fig. 4: (a-b) Water vapor concentration fields with a porosity of 0.3 (a) and 0.75 (b) and (c-d) the temperature fields with a porosity of 0.3 (c) and 0.75 (d). All simulation made based on polyurethane material with a surface absorptivity of 0.9.

The effect of porosity on the evaporation rate is shown in Fig. 5, also considering different levels of the absorptivity. In all cases, it appears that evaporation rate starts increasing linearly as the porosity increase from 0.3 to 0.6. Within this range, the increasing porosity of the BAS improves the evaporation area since it increases the water-air interface area. On the other hand, increasing the porosity decreases the second BAS layer thermal conductivity which increases the BAS surface equilibrium temperature. According to the results shown in Fig. 5, a maximum evaporation rate of 1.15 kg/(h·m^2) is obtained for a porosity of 0.75 with a surface absorptivity of 0.9 using polyurethane material. We should note that

this value slightly depends on the porosity step used in our parametric study. In our case, the parametric sweep step is of 0.02. Before the porosity reaches the optimum value, an increasing porosity contributes to a higher evaporation rate. In this region, the increase of the surface area of the water-air interface, which is the evaporation site surface area, dominates which leads to the increasing trend. The existence of an optimum and the further decrease of the evaporation rate when porosity increases after the maximum can be explained by a competition between two phenomena: the increase of porosity increases the evaporation site surface area and, in the same time, it decreases the solar radiation absorption area which is located at the surface of the BAS except at the pores location, leading eventually to a decreased surface temperature. Decreasing the photothermal surface area reduces the input energy to the system, hence the evaporation rate. We can also note that the porosity increase is expected to lead to a decrease of the BAS second layer thermal conductivity. This is actually true, but the effect is less pronounced than expected since at saturation, the porous media pores are filled with water whose thermal conductivity is almost 20 times larger than that of air.

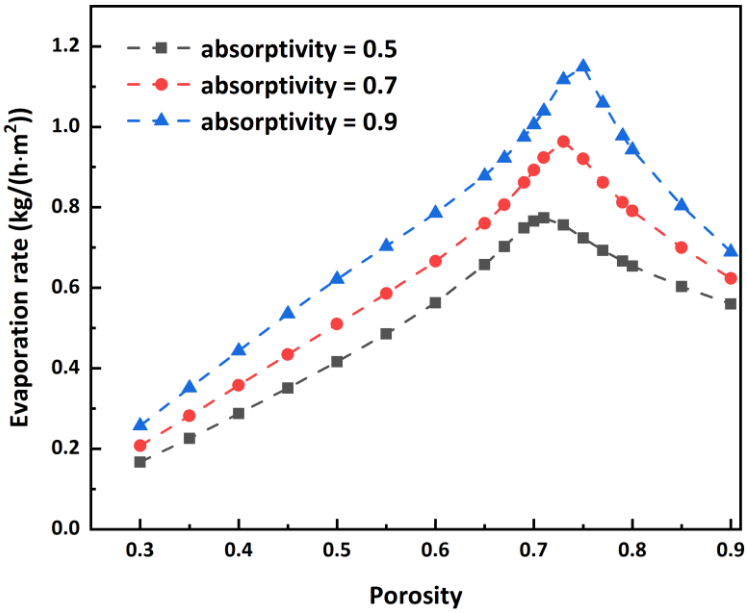

Fig. 5*:* The evaporation rate as a function of porosity.

1.5. **Effect of thermal conductivity of the BAS second layer**

We considered different bulk materials as candidates to be used for the BAS second layer in our numerical simulations including: a polymer material (Teflon), a non-metallic material (silicon) and a metallic material (aluminum) with a thermal conductivity of 0.25 W/(m·K), 130 W/(m·K) and 205 W/(m·K), respectively.

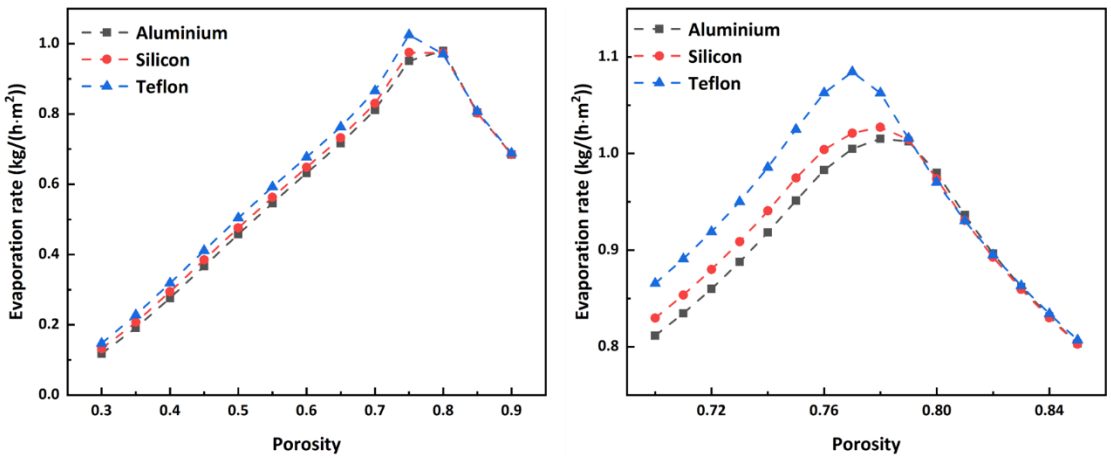

Fig. 6: (a) The evaporation rate of the BAS-enhanced SSG system as a function of porosity in the range from 0.3 to 0.9 with 3 different materials and (b) a zoom on the porosity range from 0.7 to 0.85 where the optimum is located.

Results of the evaporation rate obtained using these different materials for the second BAS layer (porous layer) are shown and compared in Fig. 6 where all materials have the same thickness equal to 5 mm. First, the evaporation rate increases linearly as the porosity increases from 0.3 to 0.7. However, we observe a small shift of the optimum position with respect to the porosity value. Comparison of the 3 materials under consideration, as can be intuitively expected, shows that Teflon, which has the smallest thermal conductivity, would be the best candidate to maximize the evaporation rate. Numerical results suggest in this case an optimal porosity of 0.77.

6. CONCLUSIONS

Theoretical modeling and numerical simulations have been conducted to study the key parameters in enhanced black absorbing sheet assisted solar steam generation. First an estimate of the asymptotic ultimate values of the mass transfer revealed that capillary flow-rate is not a limiting factor, suggesting that evaporation rate is the only key performance indicator that requires optimization. To this end, a parametric study has been conducted to assess the effect of the most relevant materials properties and environmental conditions on vapor generation rate, including the relative humidity of the ambient air, the surface absorptivity α, porosity ε and the thermal conductivity k, has been performed for optimization purposes. We show that the BAS surface absorptivity α is the key parameter in increasing the evaporation rate since it drives the energy input of the system. The evaporation rate increases linearly with α. The BAS porosity is another parameter of paramount importance to maximize the evaporation rate, whose effect is non-trivial. Interestingly, we observe a non-monotonic behavior of the evaporation rate as a function of porosity due to competing effects between evaporation sites surface area increase and solar radiation absorption sites surface area decrease when porosity increases. A maximum evaporation rate is achieved with an optimal porosity ranging between 0.7 to 0.8 and which slightly depends on the material used for the porous media and on its thermal conductivity. Obtained results can be useful for the design of optimized bilayer black absorbing sheets solar steam generators prototypes [22].

ACKNOWLEDGMENT

This work was supported by the I-SITE FUTURE Initiative (reference ANR-16-IDEX-0003) in the framework of the project NANO-4-WATER.

NOMENCLATURE

BAS	black absorbing sheet	[-]	q_{conv}	covective heat flux	[W/m.K]
ETC	effective thermal conductivity	[W/m.K]	q_{cond}	conductive heat flux	[W/m.K]
SSG	solar steam generation	[-]	q_{evap}	evaporation heat flux	[W/m.K]
k	thermal conductivity	[W/m.K]	q_{solar}	incident solar heat flux	[W/m.K]
$\dot{m}_v$	evaporation rate	[kg/s]	α	surface absorptivity	[-]
q_{abs}	absorbed radiative heat flux	[W/m²]	ε	porosity	[-]
L_v	temperature	[K]	L_v	latent heat	[kJ/kg]

REFERENCES

[1] B. Chaouchi, A. Zrelli, and S. Gabsi, *Desalination of Brackish Water by Means of a Parabolic Solar Concentrator*, Desalination **217**, 118 (2007).

[2] S. Sharma and A. Bhattacharya, *Drinking Water Contamination and Treatment Techniques*, Applied Water Science **7**, 1043 (2017).

[3] C. Tenthani, A. Madhlopa, and C. Z. M. Kimambo, *Improved Solar Still for Water Purification*, (2012).

[4] G. N. Tiwari, H. N. Singh, and R. Tripathi, *Present Status of Solar Distillation*, Solar Energy **75**, 367 (2003).

[5] L. Ye, H. You, J. Yao, and H. Su, *Water Treatment Technologies for Perchlorate: A Review*, Desalination **298**, 1 (2012).

[6] L. García-Rodríguez and C. Gómez-Camacho, *Preliminary Design and Cost Analysis of a Solar Distillation System*, Desalination **126**, 109 (1999).

[7] Y. P. Yadav, *Performance Analysis of a Solar Still Coupled to a Heat Exchanger*, Desalination **91**, 135 (1993).

[8] G. S. Dhindsa and M. K. Mittal, *Experimental Study of Basin Type Vertical Multiple Effect Diffusion Solar Still Integrated with Mini Solar Pond to Generate Nocturnal Distillate*, Energy Conversion and Management **165**, 669 (2018).

[9] P. Naveen Kumar, D. G. Harris Samuel, P. K. Nagarajan, and R. Sathyamurthy, *Theoretical Analysis of a Triangular Pyramid Solar Still Integrated to an Inclined Solar Still with Baffles*, International Journal of Ambient Energy **38**, 694 (2017).

[10] T. Arunkumar, D. Denkenberger, R. Velraj, R. Sathyamurthy, H. Tanaka, and K. Vinothkumar, *Experimental Study on a Parabolic Concentrator Assisted Solar Desalting System*, Energy Conversion and Management **105**, 665 (2015).

[11] M. A. Eltawil and Z. M. Omara, *Enhancing the Solar Still Performance Using Solar Photovoltaic, Flat Plate Collector and Hot Air*, Desalination **349**, 1 (2014).

[12] A. E. Kabeel and M. Abdelgaied, *Observational Study of Modified Solar Still Coupled with Oil Serpentine Loop from Cylindrical Parabolic Concentrator and Phase Changing Material under Basin*, Solar Energy **144**, 71 (2017).

[13] G. M. Zaki, A. Al-Turki, and M. Al-Fatani, *Experimental Investigation on Concentrator-Assisted Solar-Stills*, Solar Energy **11**, 193 (1992).

[14] G. Ni, G. Li, S. V. Boriskina, H. Li, W. Yang, T. Zhang, and G. Chen, *Steam Generation under One Sun Enabled by a Floating Structure with Thermal Concentration*, Nature Energy **1**, 1 (2016).

[15] H. Ghasemi, G. Ni, A. M. Marconnet, J. Loomis, S. Yerci, N. Miljkovic, and G. Chen, *Solar Steam Generation by Heat Localization*, Nature Communications **5**, 4449 (2014).

[16] J. B. Laurindo and M. Prat, *Numerical and Experimental Network Study of Evaporation in Capillary Porous Media. Phase Distributions*, Chemical Engineering Science **51**, 5171 (1996).

[17] J. Zhong, C. Huang, D. Wu, and Z. Lin, *Influence Factors of the Evaporation Rate of a Solar Steam Generation System: A Numerical Study*, International Journal of Heat and Mass Transfer **128**, 860 (2019).

[18] C. Hammecker, J.-D. Mertz, C. Fischer, and D. Jeannette, *A Geometrical Model for Numerical Simulation of Capillary Imbibition in Sedimentary Rocks*, Transport in Porous Media **12**, 125 (1993).

[19] R. Masoodi and K. M. Pillai, *Darcy's Law-Based Model for Wicking in Paper-like Swelling Porous Media*, AIChE Journal **56**, 2257 (2010).

[20] D. J. Bergman and D. Stroud, *Physical Properties of Macroscopically Inhomogeneous Media*, in *Solid State Physics*, Vol. 46 (Elsevier, 1992), pp. 147–269.

[21] X. H. Yang, J. J. Kuang, T. J. Lu, F. S. Han, and T. Kim, *A Simplistic Analytical Unit Cell Based Model for the Effective Thermal Conductivity of High Porosity Open-Cell Metal Foams*, Journal of Physics D: Applied Physics **46**, 255302 (2013).

[22] L. Gao, E. Nefzaoui, F. Marty, X. Wei, S. Bastide, Y. Leprince-Wang, and T. Bourouina, *Two-Dimensional Metamaterials as Meta-Foams for Optimized Surface-Enhanced Solar Steam Generation*, Solar Energy Materials and Solar Cells **243**, 111793 (2022).

[23] S. Whitaker, *Flow in Porous Media I: A Theoretical Derivation of Darcy's Law*, Transport in Porous Media **1**, 3 (1986).

[24] J.-G. Choi, D. D. Do, and H. D. Do, *Surface Diffusion of Adsorbed Molecules in Porous Media: Monolayer, Multilayer, and Capillary Condensation Regimes*, Industrial & Engineering Chemistry Research **40**, 4005 (2001).

[25] R. J. Millington and J. P. Quirk, *Formation Factor and Permeability Equations*, Nature **202**, 143 (1964).

[26] G. P. Raja Sekhar, B. S. Padmavathi, and T. Amaranath, *Complete General Solution of the Brinkman Equations*, Zeitschrift Für Angewandte Mathematik Und Mechanik **77**, 555 (1997).
[27] A. K. Datta, *Porous Media Approaches to Studying Simultaneous Heat and Mass Transfer in Food Processes. I: Problem Formulations*, Journal of Food Engineering **80**, 80 (2007).
[28] T. Tosco, D. L. Marchisio, F. Lince, and R. Sethi, *Extension of the Darcy–Forchheimer Law for Shear-Thinning Fluids and Validation via Pore-Scale Flow Simulations*, Transport in Porous Media **96**, 1 (2013).
[29] Y. Champoux and J.-F. Allard, *Dynamic Tortuosity and Bulk Modulus in Air-Saturated Porous Media*, Journal of Applied Physics **70**, 1975 (1991).
[30] V. Joekar-Niasar and S. M. Hassanizadeh, *Analysis of Fundamentals of Two-Phase Flow in Porous Media Using Dynamic Pore-Network Models: A Review*, Critical Reviews in Environmental Science and Technology **42**, 1895 (2012).
[31] M. Kaviany, *Principles of Heat Transfer in Porous Media* (Springer Science & Business Media, 2012).
[32] O. C. Zienkiewicz and T. Shiomi, *Dynamic Behaviour of Saturated Porous Media; the Generalized Biot Formulation and Its Numerical Solution*, International Journal for Numerical and Analytical Methods in Geomechanics **8**, 71 (1984).
[33] M. Liu, J. Wu, Y. Gan, D. A. Hanaor, and C. Q. Chen, *Tuning Capillary Penetration in Porous Media: Combining Geometrical and Evaporation Effects*, International Journal of Heat and Mass Transfer **123**, 239 (2018).